Journal of Applied Fluid Mechanics, Vol. 15, No. 5, pp. 1377-1386, 2022.
Available online at www.jafmonline.net, ISSN 1735-3572, EISSN 1735-3645.
https://doi.org/10.47176/jafm.15.05.1093

Numerical Study on Cubic Particle Solid–Liquid Two-Phase Flow in Multistage Pump

C. Shao[1], X. F. Wu[2†], M. G. Tan[1], H. C. Ma[3] and H. L. Liu[1]

[1] *Research Center of Fluid Machinery Engineering and Technology, Jiangsu University, Zhenjiang, Jiangsu, 212013, China*
[2]*School of Energy and Power Engineering, Jiangsu University, Zhenjiang, Jiangsu, 212013, China*
[3]*School of Mechanical Engineering, Jiangsu University, Zhenjiang, Jiangsu, 212013, China*

†*Corresponding Author Email: wxftmg@ujs.edu.cn*

(Received January 17, 2022; accepted May 30, 2022)

ABSTRACT

To investigate the movement characteristics of cubic particles in a pump, a deep-sea mining lift model pump with a specific speed of 94 is used as the research object in this study. The discrete element method is coupled with the computational fluid dynamics method to simulate the solid–liquid two-phase flow of cubic particles with different densities in the pump while the effect of particle shape on the solid–liquid two-phase flow in the pump is considered. Results show that the cubic particle movement rules for the same flow component are the same. The cubic particle density imposes a more significant effect on the number of particles in the low-velocity zone than in other zones. The number of particles in the low-velocity zone increases with the increase of density. The cubic particle velocity gradient in the impeller decreases as the particle density increases, and the particles exhibit unsatisfactory following performance in the fluid. As the density increases, the collision exhibited by the cubic particles is primarily particle-to-particle collisions, (i.e., more than 37%), and the collision rate between the cubic particles and first-stage guide vane decreases significantly. Compared with cubic particles, spherical particles are likely to obstruct the flow channel in the guide vane. The collision exhibited by the spherical particles in the pump is primarily particle-to-guide vane collision, and the collision rate between the spherical particles decreases by 15.92%.

Keywords: Numerical simulation; Spherical particles; Cubic particles; Impeller; Guide vane; Collision.

1. INTRODUCTION

The solid–liquid two-phase flow pump is an important piece of equipment for the hydraulic transportation of solid phase materials and is widely used in many fields. Because the flow of the solid–liquid two-phase flow mixture in the pump is extremely complicated, and its internal flow is difficult to visualize, numerical simulation has become an important method for analyzing the flow field in the pump (Shi and Zhu 2021).

Tarodiya and Gandhi (2019) applied a two-fluid model and a mixed model to investigate the effects of particle volume fraction and particle size on the energy performance of a slurry pump. The two-fluid model yielded results that were similar to the experimental results. The simulation results showed that the pump head and efficiency decreased with the increase of particle size and particle concentration. Zhao *et al.* (2019) analyzed the effect of sediment particle size and sediment volume fraction changes on the characteristics of an entire flow channel, and the results showed that the solid volume distribution of particles with different sizes in the impeller was the same. Wang *et al.* (2013) simulated the solid–liquid two phase flow characteristics of sand particles in a centrifugal pump using a two-fluid model. The results indicated that the particles in the impeller channel were primarily concentrated at the impeller outlet and suction side of the blade. As the particle concentration and diameter increased, the pump head and efficiency first increased and then decreased. Liu *et al.* (2009) used a two-fluid model to investigate the flow of sandy water from the Yellow River in a slurry pump. The results indicated that the most severe wear was primarily concentrated at the impeller inlet and outlet. As the particle volume fraction increased, the pump wear became more severe. The distribution of solid particles in the impeller was significantly affected by the structural parameters. Zhang *et al.* (2020) used Discrete Phase Model （DPM） and Finnie wear models to numerically calculate the internal flow and wear of a solid–liquid two-phase centrifugal pump, and the pump performance was optimized based on the response surface methodology. Li *et al.* (2012) used the DPM to analyze the following characteristics of

micro-particles in a pump. They discovered that when the particle diameter was less than 20 μm, its density did not significantly affect their follow-ability in the fluid, and its relative velocity was similar to that of the fluid. Luo and Zhang (2016) numerically simulated the wear characteristics of centrifugal slurry pumps using the DPM. The simulation results showed that the wear of the blade was primarily concentrated at the blade leading edge and the outlet of the pressure side, whereas the wear of the volute was primarily concentrated at the tongue. Datta (2012) used a two-fluid model to numerically simulate a solid–liquid two-phase flow in a deep-sea lifting pump. They discovered that the volume fraction of the solid particles was the largest near the eighth section of the volute, and it increased gradually with the increase of particle volume fraction and size. Zhang (2019) used the computational fluid dynamics–discrete element method (CFD-DEM) coupling method to investigate the law of two-phase wear in pumps. They discovered that an increase in the particle mass concentration gradually increased the pump wear rate and gradually decreased the pump wear growth rate. When the particle mass concentration exceeded 9%, the pump wear rate stabilized. Liu *et al.* (2020) investigated the effect of the volume fraction of spherical particles on the performance of deep-sea lifting pumps. The volume fraction of the particle in the impeller imposed a more significant effect on the pressure side than on the suction side. Wu *et al.* (2021) evaluated the motion law of particles in a multistage pump under different particle sizes and densities via a visual experiment. They observed that as the particle size increased, the number of particles entering the guide vane from the suction side of the guide vane decreased gradually. Meanwhile, as the particle density increased, the number of particles entering the guide vane from the suction side of the guide vane first increased and then decreased.

Currently, most studies pertaining to solid–liquid two-phase flows are based on spherical particles. However, in reality, most particles are non-spherical. Therefore, scholars have begun to investigate the effect of particle shape on pump performance. Guan *et al.* (2021) used DEM to investigate the reflux performance of non-spherical particles in a multistage pump. The results showed that the larger the departure from sphericity was, the worse the reflux performance was. Ji (2018) conducted experimental tests to investigate the movement characteristics of cylindrical particles in a single-stage centrifugal pump. The results showed that as the particle height-to-diameter ratio increased, the relative motion trajectory of the particles in the impeller shortened gradually. Mohaghegh and Udaykumar (2017) proposed a new collision algorithm for particle collisions in a viscous fluid to simulate the collisions of arbitrarily shaped particles and verified the reliability of the method through experiments. Lv (2011) used the finite element method to simulate the movement of square particles in a fluid. They discovered that the stable orientation angle of a square particle is associated with the Reynolds number of the particles when they settle in a Newtonian fluid.

Small spherical particles in single-stage pumps were primarily used in the current solid–liquid two-phase flow simulation, whereas the studies of non-spherical particle flow in multistage pumps were rare. In this study, the solid–liquid two-phase flow of cubic particles in a multistage pump was simulated using the CFD–DEM coupling method, and cubic particles with different densities were considered. In addition, the results were compared with those of spherical particles.

2. RESEARCH MODELS AND METHODS

2.1 Research model

The design parameters of the pump are as follows: rated flow Q_d= 82m^3/h; head H =20m; rotational speed n =960r/min. The model, which is a two-stage mixed-flow pump, is a hydraulic model for a deep-sea mining lift pump. A three-dimensional (3D) model of the pump is shown in Fig. 1. To obtain stable calculation result, the inlet and outlet sections of the model pump were extended appropriately. The entire calculation domain included the pump inlet extension, first-stage impeller, first-stage guide vane, secondary impeller, secondary guide vane, and pump outlet extension.

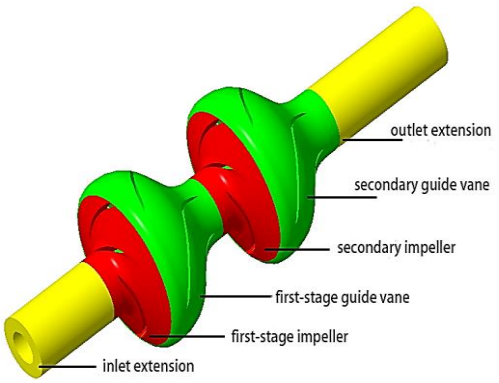

Fig. 1. 3D water model

To eliminate the effect of grid number on the simulation results, six grid schemes of different sizes were implemented. The grid quality under each scheme was controlled above 0.2, and grid independence was checked. The results are shown in Table 1.

Table 1Grid independence check

Program	Number of grids (ten thousand)	Head (m)
1	215.04	19.43
2	284.25	20.64
3	344.15	21.28
4	423.52	21.78
5	506.61	21.84
6	600.88	21.83

In Table 1, when the number of grids of the model pump reaches 4.235 million, the change in the model

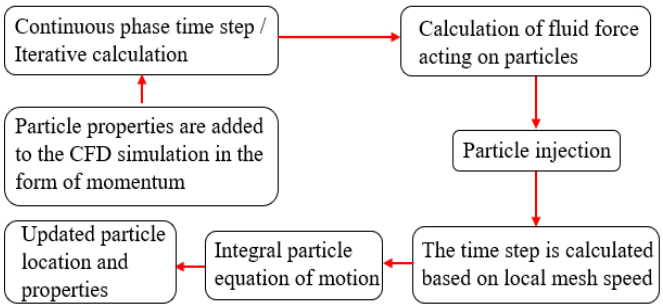

Fig. 2. CFD–DEM coupling simulation process.

pump head under different grid numbers is within 1%. Therefore, to balance the calculation time and efficiency, the fourth scheme was finally selected for simulation.

2.2 Calculation method

The CFD–DEM coupling method is based on the different mechanical properties of continuous and discrete phase media. The CFD and DEM methods were used to obtain the movement information between the flow field and solid particles. The quality, energy and momentum transfer between the solid and liquid phases were realized through coupling. This method can describe the movement of particles and flow field accurately. The coupling process is illustrated in Fig. 2. The Renormalization group (RNG) k-ε model was used in the calculations (Zhang *et al.* 2021). The wall boundary was set as no-slip (Song *et al.* 2021), the pump inlet was set to 1 atm and the outlet was set as the flow outlet.

The coupling simulation is implemented on commercial code FLUENT and EDEM.

2.3 Particle description and force

In DEM, a multi-sphere model is usually applied to construct non-spherical models (Ren *et al.* 2014). So, multiple particle models are provided in EDEM to construct the non-spherical particle models, including "single sphere", "dual sphere", "triple sphere" and "square four", as shown in Fig.3. For the sake of accuracy and simplicity (Yun and Jin 2008 and Rahul *et al.* 2010), "square four" model was applied to construct the cubic particle model, as shown in Fig.3 (e). It can be seen that the cubic particle is composed of eight spherical particles and the contact forces between cubic particles are calculated based on the interacting sphere elements.

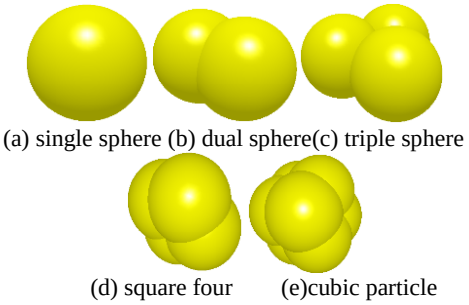

(a) single sphere (b) dual sphere(c) triple sphere

(d) square four (e)cubic particle

Fig. 3. Multiple particle models.

The Hertz-Mindlin contact model was applied to consider the interaction forces (tangential force and normal forces) between particles and between particle and wall (Lian *et al.* 2021). Collisions between particles include sphere–sphere contact, particle–sphere contact, particle–particle parallel contact, sphere–wall contact and particle–wall contact. Collisions between particle and wall include rebound behavior and rolling motion. Particle rebound behavior follows linear spring–dashpot model (Walton 1984). To consider particle rolling motion, particle-wall sliding friction coefficient was needed (Coetzee 2017). In the test, the particle-wall sliding coefficient of friction was measured and it was 0.01.

Additionally, the particles were affected by fluid during movement. The force on the particle phase was caused by the drag, gravity, pressure gradient, virtual mass, as well as Basset and Magnus forces. Typically, not all the aforementioned forces must be considered in practical problems.

Drag, gravity, and buoyancy forces are not negligible in two-phase flow calculations. For two-phase flows in pumps, Coriolis and centrifugal forces must be considered. In addition, the pressure gradient force in the pumps is not negligible. Generally, the virtual mass, as well as Saffman and Magnus forces are only valid for submicroscopic particles with a diameter of 1–10μm. Meanwhile, the Basset force must be considered only when the dimensionless frequency of fluid motion exceeds 0.5 (You *et al.* 2002). Moreover, when using CFD with the statistical approach to turbulence, such as k-ε model, the impact of turbulent fluctuating velocity on the particle motion may be of importance (depending on the particle inertia and concentration) and needs to be modeled. Here this effect was neglected for the sake of simplicity (Pozorski 2017).

Therefore, in this study, drag, gravity, buoyancy, Coriolis, centrifugal and pressure gradient forces were finally considered.

2.4 Numerical simulation scheme

The two-phase flow in the pump under the rated condition was numerically simulated. The effects of particle shape (spherical particle and cubic particle) and cubic particle density were considered.

To adhere to the principle of a single variable, the volume of a cubic particle must be the same as that

Table 2 Schemes used in current study

Scheme	Particle shape	Particle side length/ Diameter (mm)	Particle density (g/cm^3)	Particle Concentration (%)
1	Spherical, cubic	8(6.45)	1.5	3
2	Cubic	6.45	1.25, 1.5, 1.8	3

of a spherical particle. The specific schemes used are listed in Table 2.

2.5 Verification of simulation results

To verify the accuracy of the numerical method, the pump energy characteristics obtained from the simulation and test results (cubic particle density, 1.5 g/cm^3) are compared, as shown in Fig.4.

Figure 4 shows that the simulation values agree relatively well with the test values, of which the former are slightly higher than the latter. The maximum error of the head at each flow rate is 3.78%, the maximum error of efficiency is 3.72%, and the maximum error of the shaft power is 1.46%. Therefore, the numerical simulation used method in this study is reliable.

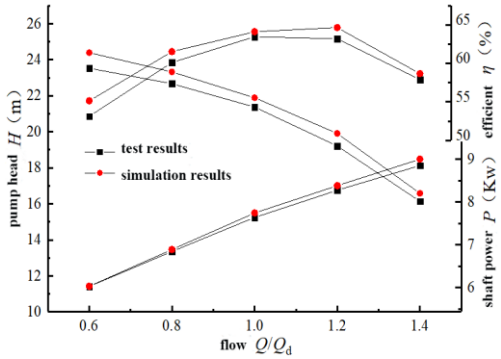

Fig. 4. Test and simulation results.

3. ANALYSIS OF CALCULATION RESULTS

3.1 Characteristics of cubic particle movement

Figure 5 shows the movement of cubic particles with a density of 1.5 g/cm^3 in the pump under the rated condition. The time interval between each figure is 0.2 s.

As shown in Fig. 5(a), at 0.2 s, the first-stage impeller and first- stage guide vanes are all filled with particles, the fastest particle reached the secondary impeller. As shown in Fig. 5(b), the entire flow channel is filled with particles at 0.4 s. The number of particles in the secondary guide vane is less than that in the first-stage guide vane. The particle volume fraction in the pump does not reach saturation. As shown in Fig. 5 (c), the particle volume in the pump becomes saturated at 0.6 s. Meanwhile, Fig. 5(d) shows that most of the particles enter the guide vane from the blade suction side of the guide vane at 0.8 s. Subsequently, the particles continue to flow along the guide vane pressure side and finally flow out along the pressure side of the guide vane.

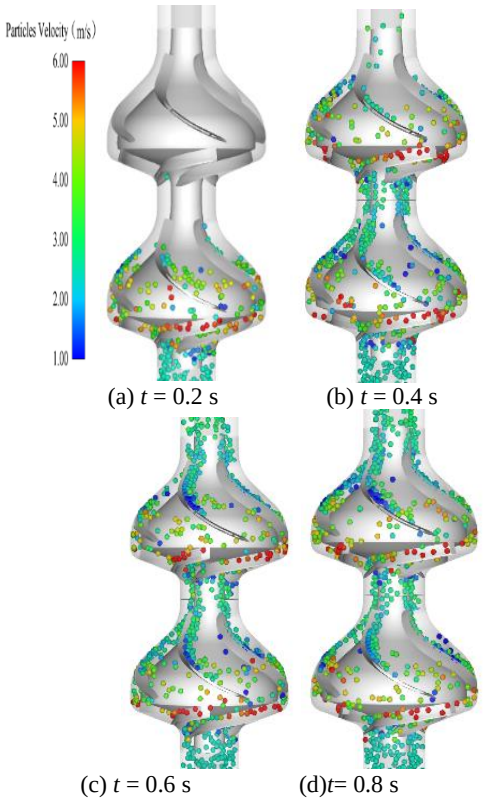

(a) t = 0.2 s (b) t = 0.4 s

(c) t = 0.6 s (d)t= 0.8 s

Fig. 5. Movement of cubic particles at different times.

In summary, at the impeller inlet, the particles are primarily distributed near the junction between the blade pressure side and hub, and the velocities are the same. In the impeller, the particle velocity increases rapidly owing to the rotation of the impeller. At the impeller outlet, most particles leave the impeller from the middle position of the blade pressure side, and the particle velocity reaches a maximum. At this point, the velocity of the particle group exceeds 6 m/s. The particle and velocity distributions in the first-stage impeller and second-stage impeller are the same. Meanwhile, the particle movements in the first-stage guide vane and second-stage guide vane are similar. This shows that the particle movement rules for the same flow component are the same, and the position of the flow component does not significantly affect particle movement.

3.2 Effect of cubic particle density on movement characteristics

3.2.1 Average velocity of cubic particles

Figure 6 shows the average velocity of cubic particles with different densities in the pump.

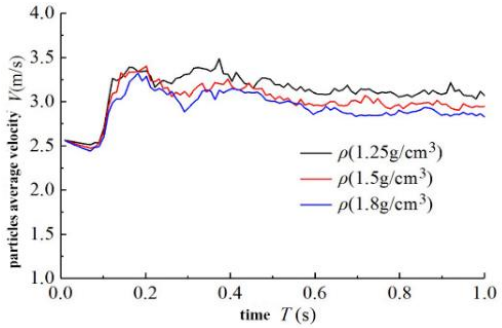

Fig. 6. Velocity of particles with different densities.

As shown, the average velocity fluctuates significantly in the initial stage, and the particle velocity gradually stabilizes. When the particle density is 1.25 g/cm^3, the average particle velocity reaches a peak of 3.39 m/s for the first time at 0.16 s, followed by a trough of 3.16 m/s at 0.22 s, and finally a peak of 3.48 m/s again at 0.37 s. Finally, the average particle velocity in the pump begins to decline and gradually stabilizes.

When the particle density is 1.5 g/cm^3, the average particle velocity reached a peak of 3.4 m/s for the first time at 0.2 s. Meanwhile, it reached a trough of 3.05 m/s for the first time at 0.3 s, followed by a peak of 3.24 m/s for the second time at 0.39 s.

When the particle density is 1.8 g/cm3, the average particle velocity reached a peak of 3.28 m/s for the first time at 0.18 s. Meanwhile, it reached a trough of 2.88 m/s for the first time at 0.29 s, followed by a peak of 3.15 m/s for the second time at 0.4 s.

As the density increased, it took a longer time for the particle average velocity to reach the second peak. Simultaneously, it also took more time for the average velocity to reach the first trough. In addition, the particle average velocity at the second peak and first trough decreased as the particle density increased. This is because the mass and inertia increase with the increase of particle density. Therefore, the particle-following performance deteriorated.

3.2.2 Cubic particle velocity distribution

Figure 7 shows the velocity distribution of cubic particles with different densities in the pump under the rated condition.

As shown, the particles velocity distribution between 2 and 3 m/s is the most. When the particle density is 1.25 g/cm^3, the particle velocity percentage between velocity 2.5 and 3 m/s is the highest, i.e., approximately 33.8%. When the particle density is 1.5 g/cm^3, the particle velocity percentage between velocity 2 and 2.5 m/s is the highest, about 32.1%. When the particle density is 1.8 g/cm^3, the particle velocity percentage between velocity 2 and 2.5 m/s is the highest at 39.0%. Under different density conditions, the particle velocity percentage between 2 and 3 m/s exceeded 50%.

It can be observed that the particle density exerts a more prominent effect on the number of particles in the low-velocity zone than in other zones. When the particle velocity exceeded 3.5 m/s, the difference in number of particles with different densities was slight. As the particle density increased, the number of particles in the low-velocity zone increased. This is because particles with higher densities maintain their motion more easily.

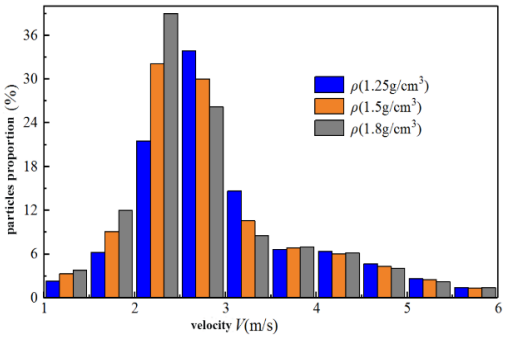

Fig. 7. Velocity distribution of particles with different densities

3.2.3 Cubic particle–liquid flow in pump

Figure 8 shows the cubic particle–liquid flow under different densities in the first-stage impeller at the rated condition.

As shown by the cases of different particle density conditions, the velocity of the fluid in the impeller increases gradually from the inlet to the outlet. The absolute velocity of the fluid in the impeller is primarily between 2 and 12 m/s. The velocity of the particle in the impeller increases gradually and ranges from 1 to 6 m/s. The particle velocity at the same position is lower than the fluid velocity because of the particle mass. The velocity gradient of the cubic particles in the impeller is similar to that of the

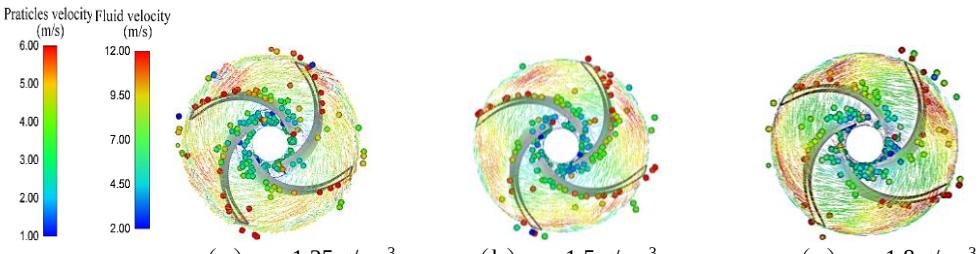

（a）ρ = 1.25 g/cm^3　（b）ρ = 1.5 g/cm^3　（c）ρ = 1.8 g/cm^3

Fig. 8. Cubic particle–liquid flow under different densities in impeller.

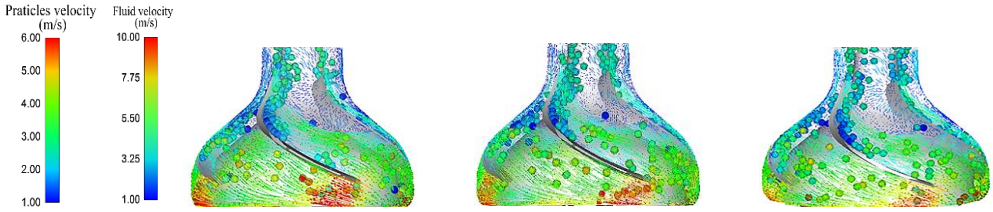

（a）ρ = 1.25 g/cm^3 （b）ρ = 1.5 g/cm^3 （c）ρ = 1.8 g/cm^3

Fig. 9. Cubic particle–liquid flow under different densities in guide vane.

liquid flow field because of the effect of fluid. From the inlet to the outlet, the particle velocity increases gradually and approaches the pressure side of the blade. Finally, most of the particles flow out of the impeller along the pressure side of the blade.

As shown in Fig. 8, the particle flow along the pressure side of the blade becomes more evident as the particle density increases. Simultaneously, the particle velocity gradient in the impeller decreases. This is because particles with a higher density have greater inertia.

Figure 9 shows the cubic particle flow under different densities in the first-stage guide vane at the rated condition.

As shown in the figure, the closer the fluid at the guide vane inlet is to the suction side, the higher is the velocity. The fluid velocity gradually decreases and the fluid is more likely to flow to the pressure side from the guide vane inlet to the outlet. The low-velocity area in the guide vane is primarily distributed on the suction side of the guide vane near the outlet owing to the flow separation. The flow direction of the particles in the guide vane is the same as that of the fluid, but the particle velocity is significantly lower than the fluid velocity. Because the fluid velocity is extremely low, almost no particle distribution occurs in the low-velocity zone.

The particle velocity distribution decreases gradually from the inlet to the outlet of the guide vane. This is primarily owing to the deceleration and pressurization of the guide vane which reduces the flow velocity in the channel, in addition to the effect of particle gravity.

The particles in the guide vane primarily accumulated from the middle to the outlet on the pressure side. This is owing to the small radius of curvature in the middle of the guide vane, and that the particles are more likely to collide with the pressure side of the guide vane at this position under the effect of the fluid.

The particle velocity gradually decreases at the same position as the particle density increases, particularly at the guide vane inlet. This is because the particle mass increases with the increase of particle density, which results in a deteriorated particle-following performance.

3.2.4 Cubic particle collision in pump

Figure 10 shows the collision rates of cubic particle in the pump under different densities, which included particle-to-particle and particle-to-flow components collisions. The rate of particle collision in a certain region is equal to the number of particle collisions in a certain region divided by the total number of particle collisions in a pump.

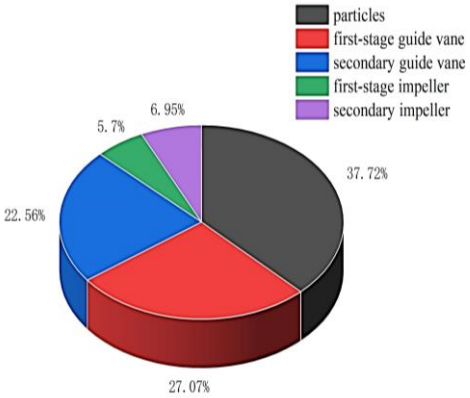

（a）ρ = 1.25 g/cm^3

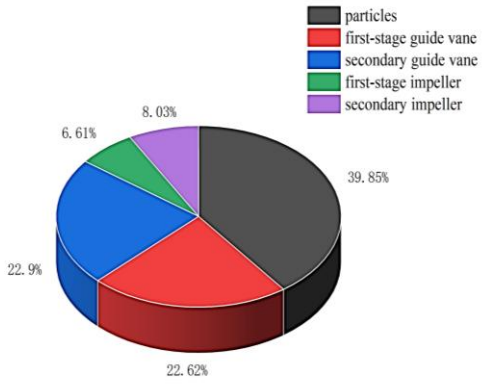

（b）ρ = 1.5 g/cm^3

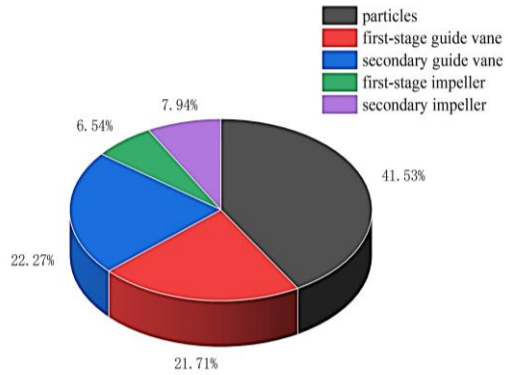

（c）ρ = 1.8 g/cm^3

Fig. 10. Collision rate of cubic particles with different densities.

The particle collision rate of the distribution was similar under different densities, and the effect of position of the flow components on the particle collision rate was insignificant. The main collision type was particle-to-particle collision, (i.e., exceeding 37%), followed by collision between particles to the guide vanes. The sum of collisions between the particles and guide vanes (first -stage vane and second-stage vane) is greater than that between the particles.

As the particle density increased, the particle-to-particle collision rate increased gradually. Meanwhile, the collision between the particles and guide vane decreased gradually. The rate of the particle-to-impeller collisions first increased and then decreased. The most significant change was observed in the collision rate between the particles and the first-stage guide vane. The collision rate between cubic particles and first-stage guide vane differed by 5.36% when particle density varies from 1.25 to 1.8 g/cm^3.

3.3 Effect of particle shape on movement characteristics

3.3.1 Particle average velocity

Figure 11 shows the average velocity of particles of different shape with a density of 1.5 g/cm^3 in the pump at the rated condition.

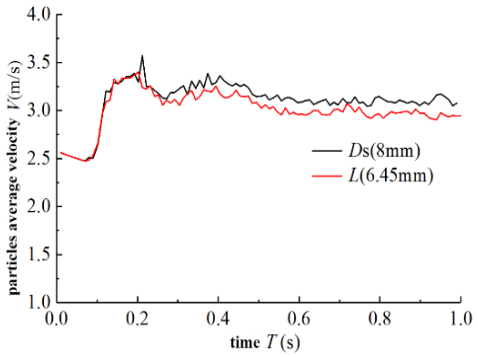

Fig. 11. Velocity of particles with different shapes.

Figure 11 shows that the average particle velocity of all particle decreases from 2.56 to 2.47 m/s within 0.1 s. This occurred because the initial velocity of the particles and fluid is the same in the inlet extension, and the drag force of the fluid on the particle is relatively low, therefore, the particles decelerate under the effect of gravity. From 0.1 to 0.22 s, the average velocity of the spherical particles increases rapidly from 2.47 to 3.54 m/s, whereas that of the cubic particles increases from 2.47 to 3.4 m/s. This phenomenon is due to the rotation of the impeller. From 0.2 to 0.3 s, the average velocity of the spherical particles decreases from 3.54 to 3.12 m/s, whereas that of the cubic particles decreases from 3.4 to 3.0 m/s. This is primarily due to the deceleration of the guide vane. Subsequently, the average velocity of the spherical and cubic particles in the pump reaches the peak at 0.38 s, and then decreases steadily. Finally, the average velocity stabilizes.

The results show that the average velocity of different-shaped particles changes similarly with time and the average velocity of different-shaped particles changes in the same manner from 0 to 0.2 s. However, after 0.2 s, the average velocity of the cubic particles is significantly lower than that of the spherical particles at the same moment. This is due to the fact that regular shape and smooth surface of the spherical particles afford better particle-following performance. Because of the edges and corners of the cubic particles, the forces on the particle surfaces are not uniform. Therefore, cubic particles exhibit unsatisfactory following performance and low velocity.

3.3.2 Particle velocity distribution in pump

Figure 12 shows the velocity distribution of different-shaped particles with a density of 1.5 g/cm^3 in the pump under the rated condition.

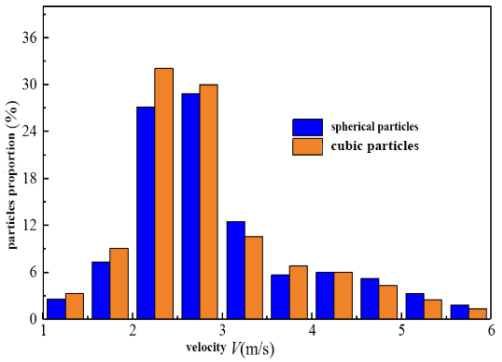

Fig. 12. Velocity distribution of different-shaped particles.

As shown, the velocity of most particles is between 2 and 3 m/s. The spherical particle velocity percentage between 2.5 and 3 m/s is the highest, i.e., 28.8%. When the particle shape is cubic, the particle velocity percentage between 2 and 2.5 m/s is the highest, i.e., approximately 32.1%. The percentage of different-shaped particles in the high velocity zone is low, because the high-velocity particles are primarily concentrated at the impeller outlet, and the impeller outlet range is small in the multistage pump.

Furthermore, the percentage of cubic particles in the low-velocity zone is significantly higher than that of spherical particles. When the particle velocity is greater than 4 m/s, the percentage of spherical particles is higher than that of cubic particles. Owing to the effect of particle shape, spherical particles with a smooth surface flow better compared with cubic particles.

3.3.3 Particle–liquid flow in pump

Figure 13 shows the spherical particle–liquid (1.5 g/cm^3) flow in the pump under the rated condition.

Compared with Fig. 8(b), Fig. 13 shows that the particle shape barely affects the fluid. As for the distribution of the different-shaped particles, the

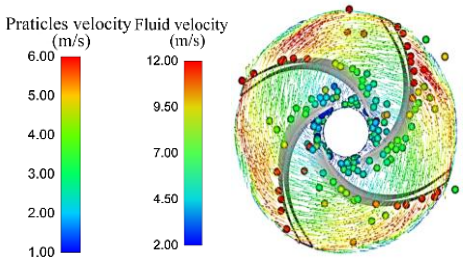

Fig. 13. Spherical particle–liquid flow in impeller.

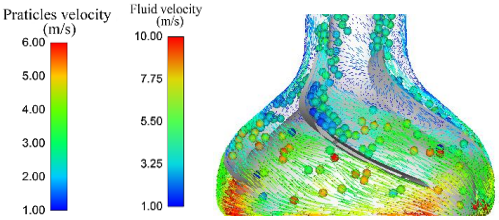

Fig. 14. Spherical particle–liquid flow in guide vane.

number of particles for both shapes in the impeller at the inlet was similar, and the distribution of the particles was relatively uniform. At the outlet of the impeller, the number of spherical particles under high-velocity movement was slightly higher than that of the cubic particles. This shows that the rotation of the impeller allows the spherical particles to receive more energy, which enables them to flow out faster.

Figure 14 shows the spherical particle–liquid flow (1.5 g/cm^3) in the guide vane under the rated condition.

Compared with the velocity and distribution of the particles presented in Fig. 9(b), Fig. 14 shows that the different-shaped particle aggregated from the middle to the outlet on the pressure side.

Compared with spherical particles, the number of cubic particles is higher on the suction side of the guide vane, which implies that cubic particles are more likely to enter the guide vane from the suction side. The number of aggregated cubic particles is significantly higher than that of spherical particles from the middle to the outlet on the pressure side. This indicates that the flow of spherical particles in the guide vane is relatively smooth, and that spherical particles are less likely to obstruct the flow channel. At the same position in the guide vane, the velocity of the spherical particles is slightly higher than that of the cubic particles, indicating that the deceleration effect of the guide vane on the cubic particles is more significant.

3.3.4 Particle collision in pump

Figure 15 shows the spherical particle collision rate based on a density of 1.5 g/cm^3 in the pump under the rated condition.

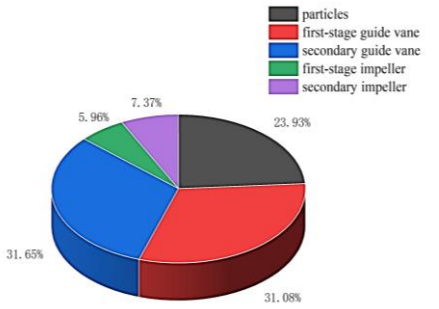

Fig. 15. Collision rate of spherical particles.

The collision of spherical particles in the pump is primarily occurs between the particles and guide vanes. The sum of collisions between the particles and guide vanes (first -stage vane and second-stage vane) is the highest at 62.73%. Meanwhile, collision between particles and particles ranks second.

Compared with Fig. 10(b), Fig. 15 shows that the proportion of particles that collide with the first-stage guide vane (first-stage impeller) is approximately equal to the proportion of particles that collide with the secondary guide vane (secondary impeller) under the same shape. The particle-to-particle and particle-to-guide vane collision rates under different shape conditions are relatively high, whereas the particle-to-impeller collision rate is relatively low.

The particle-to-particle collision rate of the spherical particles decreased by 15.92% owing to the small surface of the spherical particles under the same volume and regular shape, as compared with cubic particles, and the spherical particles propagated stably in the pump. Meanwhile, the spherical particle-to-guide vane collision rate is increased by 17.21%.

4. CONCLUSION

A solid–liquid two-phase flow was simulated using the CFD–DEM coupling method. The movement law of cubic particles and the effect of different densities were analyzed. Additionally, the effect of the particle shape in the pump was considered. The following conclusions were obtained.

1. The position of the flow component barely affected the cubic particle motion state in the multistage pump. The particles primarily accumulated from the middle to the outlet on the pressure side.

2. As the density increased, the cubic particle average velocity decreased, and the percentage of particles in the low-velocity zone increased correspondingly. The high-density cubic particles flowed slowly along the pressure side of the blade. The particle velocity decreased at the same position as the particle density increased, but did not result in more particles accumulating on the guide vane pressure side.

3. The main collision type for the cubic particle was particle-to-particle collision, and the number of

particle-to-particle collisions increased with the density.

4. Compared with the cubic particles, the spherical particles exhibited a higher average velocity and were higher in quantity at the high-velocity zone. The number of spherical particles propagating at a high-velocity was slightly higher than the number of cubic particles at the outlet of the impeller. Compared with the cubic particles, the spherical particles passed through the pressure side of the guide vane more easily.

5. The collision of spherical particles in the pump primarily occurred between the particles and guide vanes, and the rate of spherical particle-to-guide vane collision was 17.21% higher than that of cubic particle-to-guide vane collision.

ACKNOWLEDGMENTS

The authors gratefully acknowledge the support from the National Natural Science Foundation of China (No. 51979124), A Project Funded by the Program Development of Jiangsu Higher Education Institutions (PAPD).

REFERENCES

Coetzee, C. (2017). Calibration of the discrete element method. *Power Technology* 310, 104-142.

Datta, S. (2012). *Numerical investigation of flow-field inside a centrifugal slurry pump casing*. Ph.D. thesis, Jadavpur University, Kolkata, India.

Guan, Y., L. Zou, H. Zheng, Y. Bian and Z. Yu (2021). Ore particle backflow performance in the deep-sea mining slurry pump. *Journal of Harbin Engineering University* 42(11), 1557-1565.

Ji, Y. (2018). *Test and numerical simulation on coarse particles two-phase flow with in a centrifugal pump*. Master thesis, Jiangsu University, Zhenjiang, China.

Li, Y., S. Yuan, Y. Tang, P. Huang and X. Li (2012). Simulation of tracer particles movement by discrete phase model in centrifugal pump. *Transactions of the Chinese Society for Agricultural Machinery* 43(11), 113-118.

Lian, G., W. Zhong and X. Liu (2021). DEM study on the mixed feeding process of coal and cylindroid biomass particles in a screw feeder. *Advanced Powder Technology* 32(7), 2543-2554.

Liu, S., Y. Li and X. Hu (2020). Effect of Particle Volume Fraction on the Performance of Deep-sea Mining Eletric Lifting Pump Based on DEM-CFD. *Journal of Mechanical Engineering* 56(10), 257-264.

Liu, Y., A. Hui and X. Zhao (2009). Numerical calculation of interior liquid-solid two-phase flow inside a slurry pump and analysis of wear character for the impeller. *Journal of Xihua University (Natural Science Edition)* 28(2), 70-73.

Luo, L. and S. Zhang (2016). Prediction of blade wear of slurry pump based on two solid–liquid two-phase flow models. *Pump Technology* 6, 16-19.

Lv, H. (2011). *Direct numerical simulation of rectangular particle–liquid two-phase flow*. Ph.D. thesis, Chongqing University, Chongqing, China.

Mohaghegh, F. and H. Udaykumar (2017, July). Title of paper. *A Simplified Model for the Normal Collision of Arbitrary Shape Particles in a Viscous Flow. ASME 2017 Fluids Engineering Division Summer Meeting*, Waikoloa, America.

Pozorski, J. (2017). Models of turbulent flows and particle dynamics. In J.P. Minier and J. Pozorski (Ed.), *Particles in wall-bounded turbulent flows: deposition, re-suspension and agglomeration*, Cham, Switzerland, 97-150. Springer.

Rahul, B., K. Willian and H. Bruno (2010). Discrete element simulation study of a Freeman powder rheometer. *Chemical Engineering Science* 65(21), 5747-5756.

Ren, B., W. Zhong, X. Jiang, B. Jin and Z. Yuan (2014). Numerical simulation of spouting of cylindroid particles in a spouted bed. *Canadian Journal of Chemical Engineering* 92(5), 928-934.

Shi, Y. and H. Zhu (2021). Research on the Flow Characteristic in a Multi-Stage Multiphase Pump by Numerical Simulations. *Journal of Applied Fluid Mechanics* 14(2), 555-566.

Song, X., X. Mao, J. Lu and X. Zhang (2021). CFD-based optimal design of pump-turbine runner with long and short blades. *Water Resources and Hydropower Engineering* 52(4), 115-123.

Tarodiya, R. and B. Gandhi (2019). Numerical simulation of a centrifugal slurry pump handling solid–liquid mixture：Effect of solids on flow field and performance. *Advanced Powder Technology* 14(10), 2225-2239.

Walton, R. (1984). Application of molecular dynamics to macroscopic particles. *International Journal of Engineering Science* 22(8-10), 1097-1107.

Wang, J., Y. Pan, J. Zheng, C. Li and K. Kim (2013). A numerical study of the impact of find sand-particles on centrifugal pump working characteristics. *China Rural Water and Hydropower* 5, 129-132+136.

Wu, X., J. Song, K. Wang, H. Liu, H. Ye and M. Tan (2021). Visualization test on solid–liquid two-phase flow in multistage pump. *Journal of Drainage and Irrigation Machinery* 39(12), 1270-1277.

You, C., Y. Qi and X. Xu (2002). Progresses and Applications of Basset Force. *Chinese Journal of Applied Mechanics* 19(2), 31-33+139-140.

Yun, C. and O. Jin (2008). A study of influence of gravity on bulk behaviour of particulate solid. *Particuology* 6(6), 467-474.

Zhang, D., J. Mei, R. Zhao, J. Huang and Y. Jin (2020). Response surface method-based optimization of impeller of fluoroplastic two-phase flow centrifugal pump. *Journal of Drainage and Irrigation Machinery Engineering* 38(9), 898-903.

Zhang, H. (2019). *Research on particle collision and erosion mechanism in the channel of impeller*. Master thesis, Zhejiang Sci-Tech University, Hangzhou, China.

Zhang, K., M. Tan, X. Wu, H. Ma and H. Liu (2021). Clocking effect of guide vane in multi-stage centrifugal pump. *Journal of Drainage and Irrigation Machinery* 39(7), 663-670.

Zhao, X., X. Lai, G. Liao and L. Zhong (2019). Numerical Analysis of the Effects of Particle Size and Volume Fraction on the Internal Flow Field of Centrifugal Pump. *Journal of Engineering for Thermal Energy and Power* 34(4), 67-72.